Electron paramagnetic resonance and electron–nuclear double-resonance study of Ti^{3+} centres in $KTiOPO_4$

2003 J. Phys.: Condens. Matter 15 3969

(http://iopscience.iop.org/0953-8984/15/23/310)

INSTITUTE OF PHYSICS PUBLISHING JOURNAL OF PHYSICS: CONDENSED MATTER

J. Phys.: Condens. Matter **15** (2003) 3969–3984 PII: S0953-8984(03)59449-8

Electron paramagnetic resonance and electron–nuclear double-resonance study of Ti^{3+} centres in $KTiOPO_4$

S D Setzler[1], K T Stevens[2], N C Fernelius[3], M P Scripsick[4], G J Edwards[5,6] and L E Halliburton[5,7]

[1] BAE Systems, Nashua, NH 03061, USA
[2] Northrop Grumman, Space Technology, Synoptics, Charlotte, NC 28273, USA
[3] Air Force Research Laboratory, Materials and Manufacturing Directorate, AFRL/MLPSO, Wright-Patterson AFB, OH 45433, USA
[4] Nova Phase, Newton, NJ 07860, USA
[5] Department of Physics, West Virginia University, Morgantown, WV 26506, USA

E-mail: Larry.Halliburton@mail.wvu.edu

Received 11 February 2003
Published 30 May 2003
Online at stacks.iop.org/JPhysCM/15/3969

Abstract

Electron paramagnetic resonance and electron–nuclear double resonance have been used to characterize four Ti^{3+} centres in undoped crystals of potassium titanyl phosphate ($KTiOPO_4$ or KTP). These $3d^1$ defects ($S = 1/2$) are produced by ionizing radiation (either 60 kV x-rays or 355 nm photons from a tripled Nd:YAG laser), and form when the regular Ti^{4+} ions in the crystal trap an electron. Two of these trapped-electron centres are only observed in hydrothermally grown KTP and the other two are dominant in flux-grown KTP. Both of the Ti^{3+} centres in hydrothermally grown crystals have a neighbouring proton (i.e. an OH^- molecule). In the flux-grown crystals, one of the Ti^{3+} centres is adjacent to an oxygen vacancy and the other centre is tentatively attributed to a self-trapped electron (i.e. a Ti^{3+} centre with no stabilizing entity nearby). The g matrix and phosphorus hyperfine matrices are determined for all four Ti^{3+} centres, and the proton hyperfine matrix is determined for the two centres associated with OH^- ions. These Ti^{3+} centres contribute to the formation of the grey tracks often observed in KTP crystals used to generate the second harmonic of high-power, near-infrared lasers.

[6] Present address: Finnegan Henderson Farabow Garrett and Dunner LLP, Palo Alto, CA, USA.
[7] Author to whom any correspondence should be addressed.

1. Introduction

Potassium titanyl phosphate ($KTiOPO_4$ or KTP) is a widely used nonlinear optical material [1, 2]. In some applications where KTP is used to generate the second harmonic of near-infrared lasers, unwanted optical absorption bands (i.e. grey tracks) may form in the bulk of the crystal [3–7]. This effect occurs most often when intense pump beams and high repetition rates or cw operation are involved. These grey tracks appear along the beam path, and their associated absorption covers much of the visible spectrum. The induced absorption generates significant local heating which, in turn, causes severe beam distortion. Susceptibility to this bulk optical damage phenomenon varies from one KTP crystal to another, thus strongly suggesting that point defects (i.e. electron and hole traps) introduced during growth play a central role in the damage mechanism. It is important to understand the nature of the defects responsible for these absorption bands if significant progress is to be made in improving the performance of KTP-based nonlinear optical devices.

Electron paramagnetic resonance (EPR) and electron–nuclear double resonance (ENDOR) have proven to be highly effective techniques in the study of the various electron and hole traps present in KTP crystals. Roelofs [8], in an early definitive paper, used EPR to characterize four Ti^{3+} centres in flux-grown KTP crystals. Roelofs produced these centres by exposing the crystals to an electric field or by annealing in a hydrogen atmosphere. Soon thereafter, in flux-grown crystals, Andreev *et al* [9] showed that this set of four Ti^{3+} centres could be formed at room temperature using a high-power 532 nm laser beam and Andreev and Efimov [10] showed that these Ti^{3+} centres could be produced during an x-ray irradiation at room temperature. During this same period, Scripsick *et al* [11, 12] demonstrated that the dominant Ti^{3+} centres produced in hydrothermally grown crystals differed significantly (i.e. had different environments) from those observed in flux-grown crystals. These latter investigators [12] suggested that Ti^{3+} centres produced at room temperature in flux-grown crystals are adjacent to an oxygen vacancy while Ti^{3+} centres formed at 77 K in hydrothermally grown crystals are adjacent to an OH^- ion. In other studies of flux-grown KTP, Martin *et al* [13] found that thermal reduction introduced a Ti^{3+} centre different from those described by Roelofs [8], and Stevens *et al* [14] reported a Pb-related Ti^{3+} centre in doped crystals.

Additional studies have focused on the hole traps in KTP. The dominant hole-like EPR spectrum present after a 77 K x-ray or laser irradiation is assigned to a hole trapped on an oxygen ion adjacent to a potassium vacancy [15, 16]. This centre thermally decays near 160 K. Other centres in KTP have the hole (i.e. unpaired electron) trapped on an oxygen ion adjacent to an aluminium ion [10, 17] substituting for a titanium, or a silicon ion [18] substituting for phosphorus. A different type of hole-like centre occurs when a platinum atom (Pt^0) substituting for a potassium ion traps a hole and becomes a Pt^+ ion [19], or when a silver ion (Ag^+) substituting for a potassium ion traps a hole and becomes a Ag^{2+} ion [20]. Transition-metal ions such as Fe^{3+} and Cr^{3+} are also present in KTP. Scripsick *et al* [5] have suggested that a portion of the holes created at room temperature by x-rays or a laser beam in flux-grown KTP crystals will become trapped by Fe^{3+} ions on titanium sites, thus producing Fe^{4+} ions. Similar hole-trapping properties are expected for the Cr^{3+} ions.

In the present paper, we describe the results of an EPR and ENDOR investigation of the four dominant Ti^{3+} centres in undoped KTP crystals. Two of the centres were only observed in hydrothermally grown crystals and the other two centres were dominant in flux-grown crystals. We suggest that these Ti^{3+} centres play an important role in the onset of grey tracks in KTP crystals.

2. Experimental procedure

The structure [21] of KTP is orthorhombic (space group $Pna2_1$) with $a = 12.819$ Å, $b = 6.399$ Å, and $c = 10.584$ Å. This crystal has 64 atoms in the unit cell; these separate into four sets of 16 atoms which transform into each other according to the symmetry elements of the crystal. In general, the KTP lattice has two inequivalent titanium sites, two inequivalent potassium sites, two inequivalent phosphorus sites, and ten inequivalent oxygen sites. Additional information about this crystal structure is provided in [15].

The flux-grown KTP crystals used in the present investigation were provided by Crystal Associates (East Hanover, NJ). Specific growth conditions included a $K_6P_4O_{13}$ solvent and a decrease in temperature from approximately 920 to 870 °C at a rate ranging from 0.5 to 5 °C/day. The hydrothermally grown KTP crystals used in our study were provided by Synoptics (Charlotte, NC). These crystals were grown near 580 °C and are referred to by Synoptics as 'high-temperature hydrothermal'. All of the KTP samples used in our EPR and ENDOR experiments were cut from larger as-grown boules and had final dimensions of approximately $2 \times 3 \times 5$ mm^3 (with faces perpendicular to the a, b, and c crystal axes). The Ti^{3+} centres were produced by x-rays (60 kV, 30 mA, Mo target) or the third harmonic from a Nd:YAG laser (355 nm, 6 ns pulse width, 90 mJ/pulse, 10 Hz repetition rate).

The EPR and ENDOR data were obtained using a Bruker Instruments ESP-300 spectrometer operating near 9.5 GHz. Precise adjustments of the position of the microwave cavity (and the crystal) within the magnet gap were made using a horizontal section of flexible waveguide and a custom-designed unit to slightly vary the tilt of the vertical waveguide leading to the cavity. This allowed angular studies to be performed in exact high-symmetry planes of the crystal. A helium-gas-flow system was used to control the sample temperature. During the EPR measurements, the magnetic field was amplitude modulated at 25 kHz. The static magnetic field was measured with a proton gaussmeter. A small Cr-doped MgO crystal was used to correct for the difference in magnetic field between the sample and the probe tip of the gaussmeter (the isotropic g value for Cr^{3+} in MgO is taken to be 1.9800).

3. Results

The EPR signals initially present in our flux-grown and hydrothermally grown KTP crystals were attributed to varying concentrations of transition-metal ions (Fe^{3+} and Cr^{3+}). There were no EPR signals from Ti^{3+} centres in any of our KTP crystals prior to x-ray or laser irradiation. In every KTP crystal, an irradiation at 77 K produced the EPR signal near $g = 2.0$ which is assigned to the hole trapped on an oxygen ion adjacent to a potassium vacancy [15, 16]. In addition, irradiations at 77 K and at room temperature produced upwards of ten or more intense, anisotropic EPR signals having principal g values in the range from 1.95 to 1.68. Their relative intensities varied significantly from sample to sample. It is generally accepted that these signals are due to Ti^{3+} ions, with the differences in the centres being a result of the wide variety of perturbations possible in the vicinity of the titanium ion. A characteristic feature of all of these Ti^{3+} centres is an easily resolved hyperfine pattern due to several nearby 100% abundant $I = 1/2$ nuclei. In most cases, the EPR signals from the Ti^{3+} centres are best detected below approximately 60 K, as the lines become much broader at higher temperatures. Also, the majority of the Ti^{3+} centres observed in our KTP crystals are stable only below room temperature. A few of these centres, notably in flux-grown crystals, are stable at or above room temperature.

After a systematic survey of a large number of undoped KTP crystals (irradiated at 77 K or at room temperature), a consistent subset of these Ti^{3+} signals emerged as always representing

the larger concentrations, and thus being the most important. In the case of the hydrothermally grown crystals, two Ti^{3+} centres were found to dominate in the 77 K irradiated crystals, and no major Ti^{3+} centres were produced during a room-temperature irradiation. In contrast, flux-grown crystals have one Ti^{3+} centre which dominates after a 77 K irradiation and another Ti^{3+} centre which dominates after a room-temperature irradiation. These four major Ti^{3+} centres are the focus of the present investigation. Our study does not include hyperfine interactions with the ^{47,49}Ti nuclei because these lines were often obscured by the primary lines from the other weak Ti^{3+} signals. Instead, we concentrate on the hyperfine from the nearly 100% abundant neighbouring nuclei because of the information these latter interactions provide about the defect models.

For simplicity, a labelling scheme is adopted whereby Ti^{3+} centres that are only stable below room temperature are assigned a roman numeral (i.e. I, II, III, etc), while those stable at or above room temperature are assigned a letter (i.e. A, B, C, etc). In addition, a subscript (either flx or hyd) is assigned to each centre to indicate whether it is observed primarily in flux-grown or hydrothermally grown KTP crystals. Thus, we will refer in this paper to I_{hyd} and II_{hyd} centres in the hydrothermally grown crystals and to I_{flx} and A_{flx} in the flux-grown crystals. The reader should note that the Ti^{3+} centre we refer to as the A_{flx} centre is identical to Roelofs' A centre [8].

3.1. EPR spectra and analysis

When a 'high-temperature' hydrothermally grown KTP crystal is irradiated at 77 K (with either x-rays or a 355 nm laser), two dominant Ti^{3+} EPR spectra are observed at lower temperature. The EPR spectrum of centre I_{hyd} is shown in figure 1. With the magnetic field along a high-symmetry axis of the crystal, the four orientations (i.e. sites) of the Ti^{3+} defect are equivalent, and only one 'group' of EPR lines is observed. The 'stick' diagram above the data in figure 1 illustrates the contributions of four nearby nuclei (each 100% abundant with $I = 1/2$), thus accounting for the resolved hyperfine pattern. ENDOR results presented in the next section verify these hyperfine assignments. Figure 2 shows the EPR spectrum of centre II_{hyd}, the second dominant Ti^{3+} centre produced by a 77 K irradiation in a 'high-temperature' hydrothermally grown crystal. The resolved hyperfine pattern in figure 2 is explained by three inequivalent 100% abundant $I = 1/2$ nuclei (see the stick diagram). Note that neither centre I_{hyd} nor centre II_{hyd} is stable at room temperature. They both thermally decay between 140 and 200 K.

A single dominant Ti^{3+} centre appears when a flux-grown KTP crystal is irradiated at 77 K with x-rays or a 355 nm laser. This defect is labelled centre I_{flx} and its EPR spectrum is shown in figure 3. The resolved hyperfine pattern is assigned to three inequivalent 100% abundant $I = 1/2$ nuclei, as indicated by the stick diagram above the data. Centre I_{flx} becomes thermally unstable above approximately 140 K. It is important to recognize that centre I_{flx} is not one of the four Ti^{3+} centres initially reported by Roelofs [8] in flux-grown KTP crystals.

Irradiating a flux-grown KTP crystal at room temperature produces one dominant Ti^{3+} centre. This centre was initially reported by Roelofs [8] who labelled it the A centre. We refer to it as centre A_{flx}, and its EPR spectrum is shown in figure 4. There is a resolved hyperfine pattern in this EPR spectrum due to four inequivalent 100% abundant $I = 1/2$ nuclei, as illustrated by the stick diagram. Although Roelofs saw a hyperfine pattern from only two neighbouring nuclei, we are able to resolve four neighbouring contributions because of careful alignment, selection of an optimum observation temperature, and use of a reduced EPR modulation frequency. Centre A_{flx} thermally decays over a period of days to weeks when held at room temperature. If a flux-grown crystal is irradiated at 77 K and then slowly warmed, we find that the appearance of centre A_{flx} coincides with the decay of centre I_{flx} near 140 K.

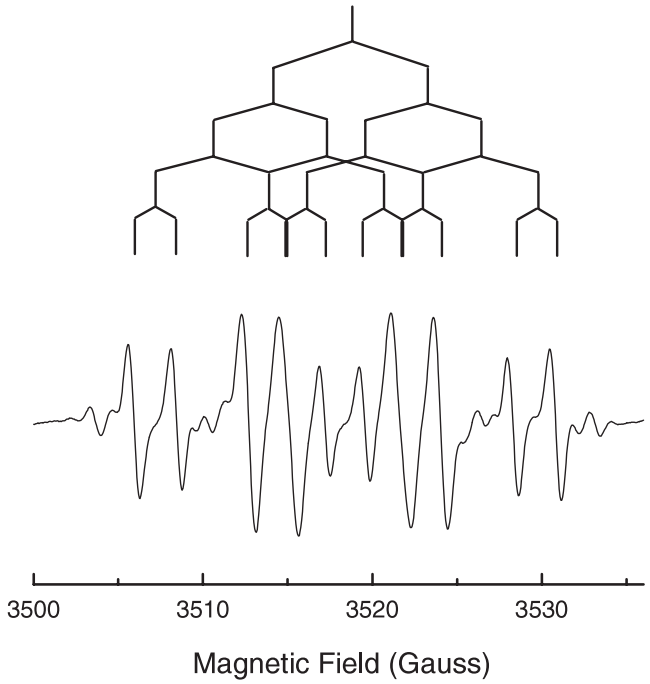

Figure 1. EPR spectrum of centre I_{hyd} taken at 30 K with the magnetic field parallel to the *a* axis. The stick diagram illustrates the four $I = 1/2$ hyperfine interactions responsible for the resolved pattern.

This suggests that the electron migrates from one trapping site to another trapping site as the temperature increases.

A complete set of angular dependence data was taken for each of these four Ti^{3+} centres. For convenience, the EPR and ENDOR spectra were acquired in a combined experiment, thus requiring the careful alignment of the magnetic field within the high-symmetry planes of the crystal to be performed only once. The *g* matrix for each Ti^{3+} centre was determined using the EPR angular dependence data plotted in figure 5. The discrete data points in figure 5 represent the magnetic field values measured at the middle of each hyperfine pattern in the EPR spectra and the solid curves were computer-generated using the 'best' values obtained for the *g* matrix. In general, for an arbitrary direction of the magnetic field, there are four magnetically inequivalent, but crystallographically equivalent, orientations (i.e. sites) for each Ti^{3+} centre. These become pairwise degenerate when the magnetic field is restricted to the *a*–*b*, *b*–*c*, and *c*–*a* planes, as shown in figure 5. Note that the expected pairwise splitting in the *c*–*a* plane is too small to be detected for centre A_{flx} (i.e. the four defect sites remain essentially degenerate as the magnetic field is rotated within this particular plane).

The experimental data in figure 5 were fitted to a spin-Hamiltonian containing only an electron Zeeman term.

$$\boldsymbol{H} = \beta \boldsymbol{S} \cdot \boldsymbol{g} \cdot \boldsymbol{B}. \tag{1}$$

In general, six parameters are required to describe a *g* matrix (i.e. three principal values and three Euler angles for the principal directions). We used a least-squares fitting program to obtain the best-fit values of the *g* matrix parameters for each of the four Ti^{3+} centres. The results are given in table 1. An EPR measurement was made at one out-of-plane orientation of the

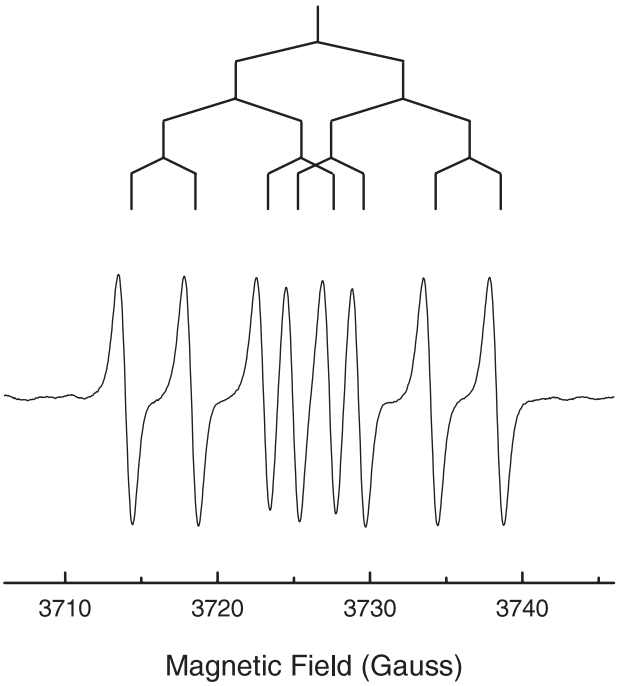

Figure 2. EPR spectrum of centre II_{hyd} taken at 30 K with the magnetic field parallel to the *a* axis. The resolved pattern is explained by three distinct $I = 1/2$ hyperfine interactions.

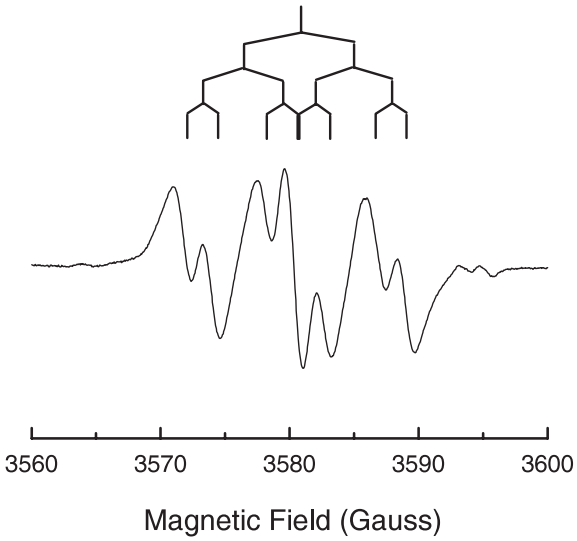

Figure 3. EPR spectrum of centre I_{flx} taken at 25 K with the magnetic field parallel to the *a* axis. Three distinct $I = 1/2$ hyperfine interactions are responsible for the resolved pattern.

magnetic field to determine the correct set of parameters for each centre, from a choice of two sets which equally well fit the in-plane data. Instead of providing Euler angles in table 1, we specify the directions of the principal axes by pairs of angles (θ, ϕ) where the polar angle

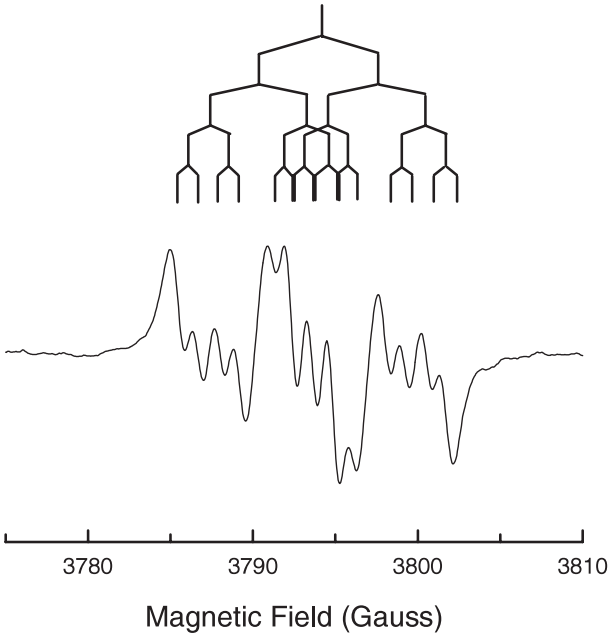

Figure 4. EPR spectrum of centre A_{flx} taken at 30 K with the magnetic field parallel to the *c* axis. The resolved pattern is explained by four distinct hyperfine interactions.

Table 1. Principal values and principal directions of the *g* matrices for the four dominant Ti^{3+} centres in KTP. Error limits on the principal values and the θ and ϕ angles are estimated to be ± 0.0005 and $\pm 0.5°$, respectively.

			Principal axes	
Centre	Principal	values	θ (deg)	ϕ (deg)
	g_1	1.7521	37.5	100.2
I_{hyd}	g_2	1.8672	59.0	241.9
	g_3	1.9383	108.9	163.7
	g_1	1.7244	40.8	33.6
II_{hyd}	g_2	1.8549	59.8	165.8
	g_3	1.9188	114.7	91.4
	g_1	1.6796	13.5	140.2
I_{flx}	g_2	1.8421	91.7	57.3
	g_3	1.9253	76.6	327.8
	g_1	1.7704	20.7	75.9
A_{flx}	g_2	1.8734	74.9	211.6
	g_3	1.9472	76.2	305.4

θ is measured relative to the *c* axis and the azimuthal angle ϕ is measured relative to the *a* axis in the *c* plane with positive rotation from *a* to *b*. The principal-axis directions given in table 1 correspond to one of the four possible sites for each Ti^{3+} centre. Applying the symmetry elements of the lattice will generate the principal-axis directions for the other three sites (see [15] for the appropriate expressions).

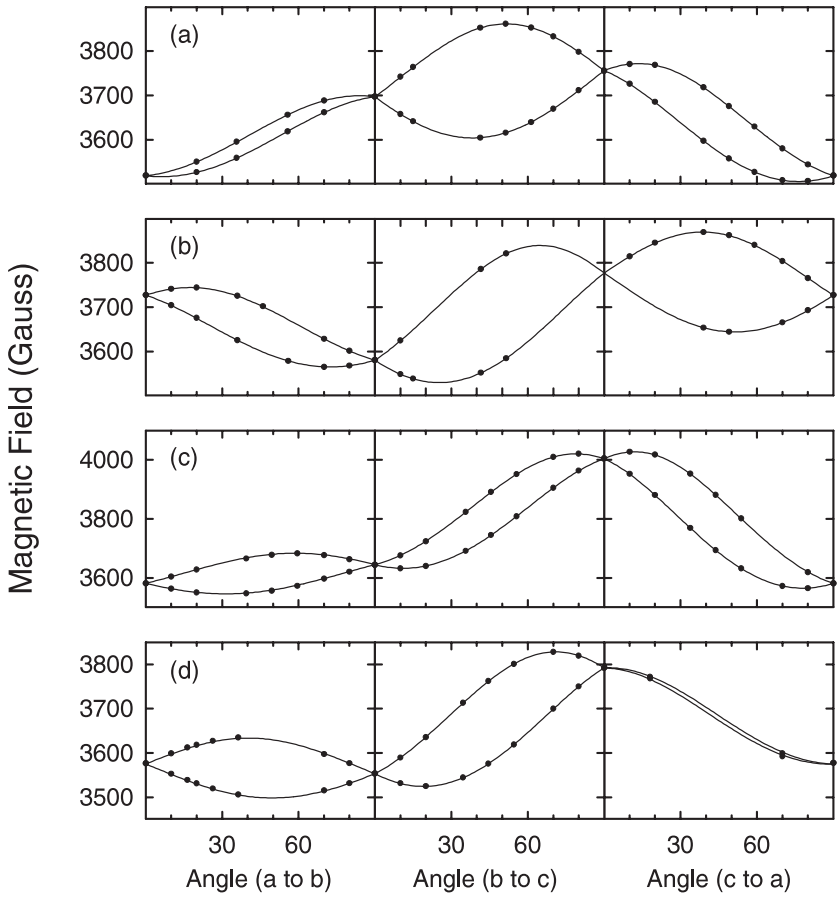

Figure 5. Angular variation associated with the g matrix of each Ti^{3+} centre. Hyperfine splittings are not included. Data for centres I_{hyd}, II_{hyd}, I_{flx}, and A_{flx} are shown in (a), (b), (c), and (d), respectively.

3.2. ENDOR spectra and analysis

A complete set of ENDOR data was acquired for each nucleus contributing to the hyperfine patterns associated with the Ti^{3+} centres. Figure 6 shows the ENDOR spectrum for centre I_{hyd}. Stick diagrams above the ENDOR data indicate the larger interactions, corresponding in this case to three pairs of ^{31}P lines and one pair of ^{1}H lines. The pair of proton ENDOR lines and the lowest frequency pair of phosphorus lines are centred on the 'free' nuclear resonance frequency ν_N (where $\nu_N = g_N\beta_N B/h$) and separated by the hyperfine interaction A. Conversely, the remaining two ^{31}P pairs in figure 6 are centred on $A/2$ and separated by $2\nu_N$. From the EPR data in figure 1, we see that centre I_{hyd} has four large hyperfine interactions. And now from the ENDOR data in figure 6 (taken with the same orientation of magnetic field), we see that a ^{31}P nucleus is responsible for the largest of these interactions, another ^{31}P and a ^{1}H are responsible for the two similar intermediate interactions, and a third ^{31}P is responsible for the smallest of the four interactions. Additional lines representing weak interactions can be observed in figure 6, but they are not analysed in the present study.

An ENDOR spectrum from centre A_{flx} is shown in figure 7. The stick diagrams above the data show four hyperfine interactions, which agree with the EPR spectrum in figure 4 (also

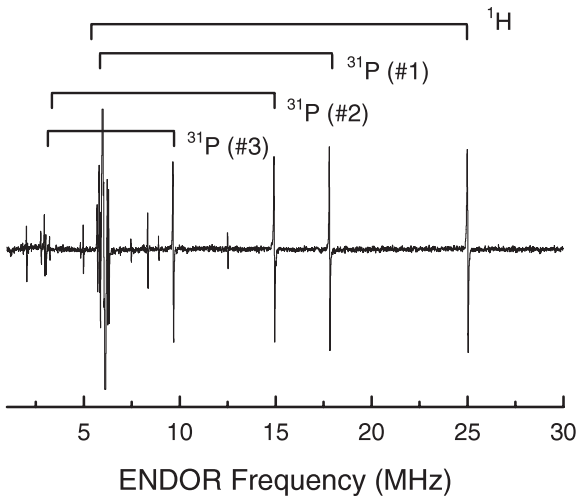

Figure 6. ENDOR spectrum of centre I_{hyd} taken at 10 K with the magnetic field parallel to the *a* axis. The stick diagram illustrates the three pairs of lines arising from ^{31}P nuclei and the one pair of lines arising from a proton.

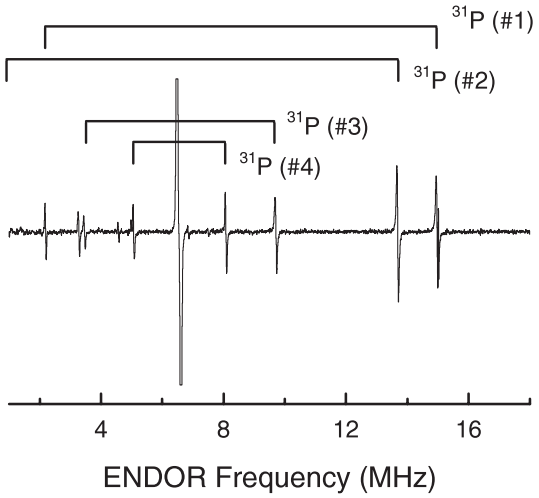

Figure 7. ENDOR spectrum of centre A_{flx} taken at 13 K with the magnetic field parallel to the *c* axis. The stick diagram illustrates the four pairs of lines arising from ^{31}P nuclei.

taken with the magnetic field along the *c* axis). For centre A_{flx}, all four interactions are with ^{31}P nuclei. Two of these ^{31}P interactions in figure 7 are represented by pairs of lines centred on $A/2$ and separated by $2\nu_N$, and the other two have pairs of lines centred on ν_N and separated by A.

The angular dependence of the ENDOR spectra was obtained for each Ti^{3+} centre. As a representative example of these results, the data from centre I_{hyd} are shown in figure 8. Since the identity of each participating nucleus is known, we only plot the high-frequency ENDOR lines from each of the four nuclei representing the largest hyperfine interactions (see figure 6). The ENDOR lines in the 22–29 MHz region are due to a ^{1}H nucleus, and the remaining lines at lower frequency are due to three ^{31}P nuclei. Note that these ENDOR results in figure 8

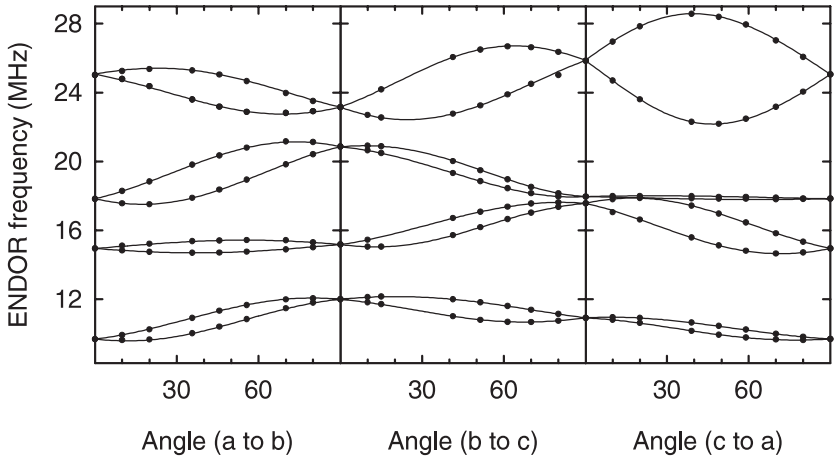

Figure 8. Angular dependence of the ENDOR spectrum of centre I_{hyd}. Only the high-frequency component of each of the four ENDOR pairs is shown.

contain information about the anisotropy of both the g matrix and the hyperfine matrices (i.e. a different magnetic field was used for each of the angles where ENDOR data were taken). We have fitted the data in figure 8 using the following spin-Hamiltonian and the appropriate $g_N\beta_N$ value for protons and phosphorus.

$$\boldsymbol{H} = \beta \boldsymbol{S} \cdot \boldsymbol{g} \cdot \boldsymbol{B} + \boldsymbol{I} \cdot \boldsymbol{A} \cdot \boldsymbol{S} - g_N \beta_N \boldsymbol{I} \cdot \boldsymbol{B}. \tag{2}$$

Each of the four hyperfine matrices was determined separately. The parameters describing the g matrix were not allowed to vary during these fitting runs (i.e. the g matrix was fixed at the values given in table 1). An ENDOR measurement was made at one out-of-plane orientation of the magnetic field to determine the correct set of parameters for each hyperfine matrix, from a choice of two sets which equally well fit the in-plane data. The results for centre I_{hyd} are given in table 2, and the solid curves in figure 8 were generated using these 'best' values for the parameters. Final sets of hyperfine values for centres II_{hyd}, I_{flx}, and A_{flx} are also given in table 2.

4. Discussion

The titanium ions in KTP crystals prefer to be in the Ti^{4+} state. These ions will, however, trap an electron and convert to the Ti^{3+} state during an exposure to ionizing radiation (i.e. either x-rays or an intense laser beam) or during application of an electric field at elevated temperature. There are two general mechanisms which allow the extra electron to be stabilized at a titanium ion. The often occurring mechanism is to have a neighbouring defect with an 'effective' positive charge, relative to the lattice, serve as the stabilizing entity. In KTP, these nearby defects could be OH^- molecular ions, oxygen vacancies, or divalent cations substituting for potassium ions. Because of the complicated crystal structure of KTP, it is easy to see that a rich variety of Ti^{3+} centres could form when one takes into account the different stabilizing entities and their large number of possible positions relative to the paramagnetic ion. The second mechanism to stabilize an electron on a titanium ion is referred to as 'self-trapping'. In this case, there is no need for a nearby charged defect; instead, the presence of the extra electron induces a lattice relaxation of the surrounding ions which in turn forms a local potential well sufficiently deep to hold the electron at that particular titanium site.

Table 2. Principal values and principal directions of the hyperfine matrices for four Ti^{3+} centres in KTP. Error limits for the principal values and the θ and ϕ angles are estimated to be ± 0.02 MHz and $\pm 0.5^\circ$, respectively.

Centre	Nucleus	Principal values (MHz)		Principal axes θ (deg)	Principal axes ϕ (deg)
I_{hyd}					
		A_1	13.87	44.0	323.2
	^1H	A_2	14.09	98.6	242.1
		A_3	26.37	47.3	160.1
		A_1	22.84	80.6	162.6
	^{31}P(#1)	A_2	22.94	9.7	329.0
		A_3	29.54	92.2	252.3
		A_1	17.01	94.2	300.3
	^{31}P(#2)	A_2	17.22	66.3	28.5
		A_3	23.05	24.1	219.8
		A_1	6.89	77.0	188.4
	^{31}P(#3)	A_2	8.10	28.5	73.3
		A_3	12.03	65.1	284.5
II_{hyd}					
		A_1	9.76	133.7	122.8
	^1H	A_2	10.71	63.9	184.9
		A_3	22.61	125.0	254.9
		A_1	22.15	19.7	86.4
	^{31}P(#1)	A_2	22.32	108.9	70.1
		A_3	28.38	95.1	161.8
		A_1	16.36	4.8	130.5
	^{31}P(#2)	A_2	16.53	92.5	71.3
		A_3	23.54	94.1	161.5
I_{flx}					
		A_1	22.12	95.2	304.0
	^{31}P(#1)	A_2	22.24	62.9	31.3
		A_3	29.15	27.7	224.0
		A_1	16.61	73.7	172.2
	^{31}P(#2)	A_2	16.74	17.1	334.4
		A_3	23.45	95.0	260.8
		A_1	5.29	72.2	190.7
	^{31}P(#3)	A_2	6.49	149.0	248.5
		A_3	10.04	65.5	289.2
A_{flx}					
		A_1	16.58	10.5	160.5
	^{31}P(#1)	A_2	16.75	89.4	253.9
		A_3	23.36	100.4	164.0
		A_1	14.28	2.0	335.9
	^{31}P(#2)	A_2	14.68	90.0	244.8
		A_3	21.37	88.0	154.8
		A_1	3.74	76.6	147.8
	^{31}P(#3)	A_2	4.24	121.2	229.6
		A_3	7.23	34.5	258.1
		A_1	0.84	76.0	146.8
	^{31}P(#4)	A_2	1.40	56.8	47.4
		A_3	3.94	36.8	256.4

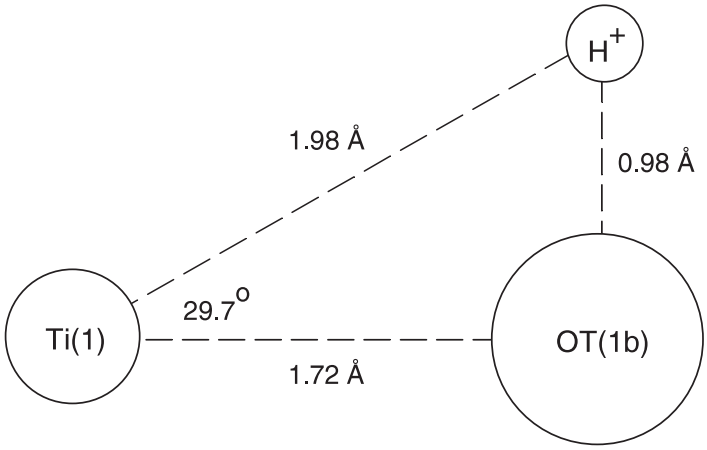

Figure 9. Schematic representation showing a possible location of the proton for centre I_{hyd}. The unpaired electron is localized on Ti(1) and the proton and OT(1b) combine to form an OH^- ion.

4.1. Models of Ti^{3+} centres in hydrothermal KTP

Two of our Ti^{3+} defects, centres I_{hyd} and II_{hyd}, are observed only in hydrothermally grown KTP crystals. And, from the ENDOR results, we see that these two centres have a nearby proton stabilizing the Ti^{3+} ion. In an oxide crystal, such as KTP, the protons bond with oxygen ions to form OH^- molecular ions. Furthermore, it is well known that KTP crystals grown by the hydrothermal technique have much larger concentrations of OH^- ions than crystals grown by the flux technique [22, 23]. These protons are necessary to charge-compensate potassium vacancies in hydrothermally grown KTP crystals.

The anisotropic portion of each hyperfine matrix provides information about the dipole–dipole interaction between the unpaired electron, localized primarily on the titanium ion, and the specific nearby nucleus. The hyperfine matrices for centres I_{hyd} and II_{hyd} are nearly axial, and their unique axes can provide information about the directions from the unpaired electron (i.e. the titanium site) to the various nuclei. By comparing these unique axes to crystallographic data, it is possible to suggest, for each centre, which crystallographically inequivalent titanium site is occupied by the Ti^{3+} ion. To aid in this process, the coordinates of the ions surrounding the two crystallographically inequivalent titanium ions in the KTP lattice are given in table 3. Following Thomas *et al* [21], we refer to these titanium sites as Ti(1) and Ti(2). The first set of 13 entries in table 3 describes the cluster of ions having Ti(1) at the centre. The oxygen ions listed in the set are the six nearest neighbours to Ti(1), while the phosphorus ions listed are the next neighbours to four of these oxygens. Also included are titanium next neighbours. Within the labelling parenthesis accompanying each ion, the 1 denotes ions surrounding Ti(1) and the lower-case letters distinguish between the various ions in the same category. The second set of 13 entries in table 3 describes, in a similar manner, the cluster of ions surrounding Ti(2). When searching for possible correlations between principal-axis directions and ion-to-ion directions, it is important to include the principal-axis directions for all four symmetry-related sites of a given centre, as well as parallel and anti-parallel directions for each principal axis.

When comparing the directions of principal axes in table 2 with the crystal structure information in table 3, we find good agreement for centre I_{hyd} if the Ti^{3+} ion is located at the Ti(1) ion site. The Ti(1)–P(1b) direction is 5.7° away from the $^{31}P(\#1)$ unique axis and the Ti(1)–P(1a) direction is 11.2° away from the $^{31}P(\#2)$ unique axis. A clear correlation could

Table 3. Positions of ions in the KTP lattice given in units of the a, b, and c lattice parameters. The first set of 13 ions have Ti(1) at the centre and the second set of 13 have Ti(2) at the centre. These values were obtained from data in [21] after applying, in some cases, symmetry operations of the crystal.

Ion	x/a	y/b	z/c
Ti(1)	0.3729	0.5001	0.9996
O(1a)	0.4859	0.4867	0.8497
O(1b)	0.3874	0.8106	0.9585
O(1c)	0.4897	0.5343	1.1170
O(1d)	0.3887	0.1918	1.0117
OT(1a)	0.2752	0.4653	0.8561
OT(1b)	0.2768	0.5413	1.1097
P(1a)	0.4981	0.3363	0.7397
P(1b)	0.3192	1.0020	0.9872
P(1c)	0.5019	0.6637	1.2397
P(1d)	0.3192	0.0020	0.9872
Ti(1a)	0.2466	0.2695	0.7484
Ti(1b)	0.2534	0.7695	1.2484
Ti(2)	0.2466	0.2695	0.7484
O(2a)	0.4004	0.1986	0.7208
O(2b)	0.0934	0.3070	0.7589
O(2c)	0.2475	0.0402	0.8718
O(2d)	0.2528	0.4619	0.6008
OT(2a)	0.2752	0.4653	0.8561
OT(2b)	0.2232	0.0413	0.6097
P(2a)	0.4981	0.3363	0.7397
P(2b)	−0.0019	0.1637	0.7397
P(2c)	0.3192	0.0020	0.9872
P(2d)	0.1808	0.5020	0.4872
Ti(2a)	0.3729	0.5001	0.9996
Ti(2b)	0.1271	0.0001	0.4996

not be found between the hyperfine unique axis for the ^{1}H interaction and a crystallographic ion-to-ion direction. Given that the average length of an O–H bond is 0.98 Å, and the average Ti–O bond length at the Ti(1) site is 1.97 Å, there are a number of possible choices for the location of the proton relative to the Ti(1) ion. Nevertheless, we suggest, with some caution, that the proton may be bound to OT(1b). Figure 9 shows a proton 0.98 Å from the OT ion, yielding an OT(1b)–Ti(1)–H angle of 29.7°, in good agreement with the 23.3° deviation of the ^{1}H unique hyperfine axis from the Ti(1)–OT(1b) bond direction. The separation distance of 1.98 Å in figure 9 also matches exactly the separation distance of 1.98 Å predicted by a simple dipole–dipole calculation.

In the case of centre II_{hyd}, there is good agreement for the two ^{31}P interactions if the Ti^{3+} ion is located at the Ti(2) ion site. The Ti(2)–P(2a) direction is 11.2° away from the ^{31}P(#1) unique axis and the Ti(2)–P(2b) direction is 8.6° away from the ^{31}P(#2) unique axis. And, invoking the argument used earlier for centre I_{hyd}, it appears likely that the proton in centre II_{hyd} is bound to either OT(2a) or OT(2b).

4.2. Models of Ti^{3+} centres in flux KTP

Proton hyperfine interactions are not observed in the ENDOR spectra of centres I_{flx} and A_{flx}, which suggests that the unpaired electron must be self-trapped on the titanium ion or there

must be either an adjacent oxygen vacancy or a divalent impurity on a neighbouring potassium site. Since centre I_{flx} becomes unstable near 140 K while centre A_{flx} is stable for days or weeks at room temperature, the models proposed for these two centres must be different (i.e. they must have different stabilization mechanisms).

Earlier investigators have suggested that centre A_{flx} is associated with an oxygen vacancy [5, 12]. In this scenario, an oxygen vacancy provides charge compensation for two potassium vacancies in the as-grown flux crystal (i.e. an O^{2-} ion is missing along with two K^+ ions). The vacancy (i.e. missing oxygen) is located between two titanium ions and initially has an effective charge of 2+. When free electrons and holes are produced by an intense laser beam or x-rays, an electron will be trapped at the oxygen vacancy. This trapped electron is localized on one of the two adjacent titanium ions, thus forming a Ti^{3+} paramagnetic ion. Localizing the unpaired electron on one of the titanium neighbours instead of having it shared equally by the two titanium neighbours is analogous to the behaviour previously observed for the E_1' centres in crystalline SiO_2 [24].

Roelofs [8] and others [9, 10] have observed a set of four Ti^{3+} centres which are stable at room temperature in flux-grown KTP (centres B, C, and D, in addition to centre A described in the present investigation). An oxygen-vacancy assignment can account for these four centres. There are two inequivalent titanium sites, and if we restrict the vacancy to be one of the two adjacent OT oxygen sites, then there are four distinctly different configurations of the combined Ti^{3+} ion and OT vacancy in the KTP lattice. The experimentally observed relative concentrations of these four centres are not equal, which means that the unpaired electron will probably hop across the oxygen vacancy (over a barrier) from one titanium to another to produce a thermal equilibrium distribution of the four centres. Support for the oxygen-vacancy assignment for centre A_{flx} comes from the fact that Roelofs [8] saw the set of four centres after subjecting a flux sample to a reducing treatment in hydrogen. Even stronger evidence for the oxygen-vacancy assignment was provided by a recent experiment in which we produced centre A_{flx} in hydrothermally grown KTP by heating the crystal in a nitrogen atmosphere for 4.5 h at 800 °C and then irradiating with x-rays at room temperature. Our result suggests that oxygen vacancies were introduced into the hydrothermally grown crystal during the reduction. These latter crystals do not normally contain oxygen vacancies (since there are usually more than enough protons, present in the form of OH^- ions, to charge-compensate all of the potassium vacancies).

Turning to centre I_{flx}, we suggest that this Ti^{3+} ion must represent a self-trapped electron or be associated with a neighbouring divalent cation (e.g. Mg^{2+}, Ca^{2+}, Sr^{2+}, etc) substituting for a K^+ ion. It is difficult to distinguish between these two models on the basis of magnetic resonance evidence since the most likely divalent cations have no appreciable abundance of magnetic isotopes to give observable hyperfine splittings. Even if present, hyperfine interactions with these divalent cations would be weak because of their large distance from the unpaired electron on the titanium. Without hyperfine evidence, there can be no final conclusions about the correct model. We believe, however, that sufficient evidence does exist to strongly suggest that centre I_{flx} is a self-trapped electron (i.e. a Ti^{3+} ion with no stabilizing entity nearby).

We have found that irradiating a flux-grown crystal at 77 K results in a large concentration of I_{flx} centres and very few, if any, A_{flx} centres. This result is less likely to occur if centre I_{flx} is associated with a divalent cation because the radiation-induced 'free' electrons will move through the lattice and have reasonable probabilities of being trapped by either a divalent cation or an oxygen vacancy. Thus, we would expect significant concentrations of both I_{flx} and A_{flx} centres to be created at 77 K. However, if centre I_{flx} is a self-trapped electron, then many more I_{flx} centres than A_{flx} centres are expected to be created when a flux-grown crystal is irradiated

at 77 K. This is because of the greatly increased number of potential trapping sites for the electron. Every unperturbed titanium ion in the crystal could potentially self-trap an electron and form centre I_{flx} (i.e. the number of unperturbed titanium sites is much greater than the number of oxygen vacancies). A final question concerns the inability to form centre I_{flx} in hydrothermally grown crystals. We suggest that the extremely large concentration of protons in these crystals limits the number of unperturbed titanium sites and thus prevents centre I_{flx} from being formed. Basically, the concentrations of protons in these crystals is such that all titanium ions are within four or five lattice spaces of a proton.

When comparing the directions of the principal axes with the crystal structure information (in table 3), we find good agreement for centre I_{flx} if the Ti^{3+} ion is located at the Ti(1) site. The Ti(1)–P(1a) direction is 10.0° away from the ^{31}P(#1) unique axis and the Ti(1)–P(1b) direction is 4.0° away from the ^{31}P(#2) unique axis. In the case of centre A_{flx}, we find good agreement if the Ti^{3+} ion is located at the Ti(2) site. Specifically, the Ti(2)–P(2a) direction is 12.2° away from the ^{31}P(#1) unique axis for centre A_{flx}, the Ti(2)–P(2b) direction is 13.2° away from the ^{31}P(#2) unique axis, the Ti(2)–P(2d) direction is 9.0° away from the ^{31}P(#3) unique axis, and the Ti(2)–P(2c) direction is 10.0° away from the ^{31}P(#4) unique axis.

5. Summary

Four distinct Ti^{3+} centres have been studied in undoped single crystals of KTP. Two of these (centres I_{hyd} and II_{hyd}) are present in hydrothermally grown material and two (centres I_{flx} and A_{flx}) are present in flux-grown material. Centres I_{hyd} and II_{hyd} have the Ti^{3+} ion occupying the inequivalent Ti(1) and Ti(2) crystal sites, respectively, and they each have a proton bonded to an adjacent oxygen (OT) ion. These protons, in the form of OH^- ions, provide the stabilizing influence to hold the unpaired electron at the titanium site. Centre A_{flx} is a Ti^{3+} ion located adjacent to an oxygen vacancy (i.e. a missing OT ion) and is the most stable of the four centres investigated. The other centre observed in flux-grown material, centre I_{flx}, is suggested to be a self-trapped electron. We note that further investigation is needed to verify this last assignment.

Identification of the stabilizing mechanism for each of the different Ti^{3+} centres formed in undoped KTP helps to explain why grey tracks form in some crystals and not in others. It is now well established that significant concentrations of potassium vacancies are present in all KTP crystals (both hydrothermally grown and flux-grown). These K^+ vacancies are charge-compensated, in large part, by OH^- molecular ions in the hydrothermally grown crystals and by oxygen vacancies in the flux-grown crystals. During exposure to x-rays or an intense laser beam, these same entities (the OH^- ions or oxygen vacancies) act as stabilizers for the Ti^{3+} centres. The thermal stability of each Ti^{3+} centre depends on the nature of its specific stabilizing entity (e.g. centres I_{hyd} and II_{hyd} in hydrothermally grown KTP are considerably less stable than centre A_{flx} in flux-grown KTP). In general, crystals in which larger concentrations of the more stable Ti^{3+} centres can be produced may be expected to have a greater susceptibility to grey tracking. Equally important, the nature and concentration of hole traps (impurities such as silicon, platinum, iron, chromium, etc) in a particular KTP crystal may significantly affect its resistance to bulk optical damage.

Acknowledgments

This research was supported at West Virginia University by the Air Force Office of Scientific Research under Grants F49620-96-1-0452 and F49620-00-1-0301. The authors wish to thank G M Loiacono and R F Belt for providing the KTP samples.

References

[1] Koechner W 1999 *Solid-State Laser Engineering* 5th edn (Berlin: Springer)
[2] Dmitriev V G, Gurzadyan G G and Nikogosyan D N 1999 *Handbook of Nonlinear Optical Crystals* 3rd edn (Berlin: Springer)
[3] Blachman R, Bordui P F and Fejer M M 1994 *Appl. Phys. Lett.* **64** 1318
[4] Boulanger B, Fejer M M, Blachman R and Bordui P F 1994 *Appl. Phys. Lett.* **65** 2401
[5] Scripsick M P, LoIacono D N, Rottenberg J, Goellner S H, Halliburton L E and Hopkins F K 1995 *Appl. Phys. Lett.* **66** 3428
[6] Feve J P, Boulanger B, Marnier G and Albrecht H 1997 *Appl. Phys. Lett.* **70** 277
[7] Scripsick M P and Ruland G E 1998 *OSA Trends in Optics and Photonics, Advanced Solid State Lasers* vol 19, ed W R Bosenberg and M M Fejer (Washington, DC: Optical Society of America) pp 85–9
[8] Roelofs M G 1989 *J. Appl. Phys.* **65** 4976
[9] Andreev B V, Maslov V A, Mikhailov V A, Pak S K, Shaunin O P and Sherbakov I A 1991 *SPIE Proc.* **1839** 280
[10] Andreev B V and Efimov V N 1992 *Mod. Phys. Lett.* B **6** 177
[11] Scripsick M P, Edwards G J, Halliburton L E and Belt R F 1991 *J. Appl. Phys.* **70** 2991
[12] Scripsick M P, Edwards G J, Halliburton L E, Belt R F and Loiacono G M 1994 *J. Appl. Phys.* **76** 773
[13] Martin M J, Bravo D, Sole R, Diaz F, Lopez F J and Zaldo C 1994 *J. Appl. Phys.* **76** 7510
[14] Stevens K T, Halliburton L E, Roth M, Angert N and Tseitlin M 2000 *J. Appl. Phys.* **88** 6239
[15] Edwards G J, Scripsick M P, Halliburton L E and Belt R F 1993 *Phys. Rev.* B **48** 6884
[16] Laruhin M A, Efimov V N and Nazarova V A 1997 *Appl. Magn. Reson.* **12** 517
[17] Yu J T, Lee C H, Liu K T, Liu C L, Huang Y, Payne D A and Lii K H 1995 *J. Phys. Chem. Solids* **56** 233
[18] Stevens K T, Setzler S D, Halliburton L E, Scripsick M P and Rottenberg J 1999 *J. Appl. Phys.* **85** 1063
[19] Garces N Y, Stevens K T and Halliburton L E 2000 *J. Appl. Phys.* **87** 8682
[20] Garces N Y 2001 *PhD Dissertation* West Virginia University
[21] Thomas P A, Glazer A M and Watts B E 1990 *Acta Crystallogr.* B **46** 333
[22] Loiacono G M, Loiacono D N, McGee T and Babb M 1992 *J. Appl. Phys.* **72** 2705
[23] Morris P A, Crawford M K and Jones B 1992 *J. Appl. Phys.* **72** 5371
[24] Weil J A 1984 *Phys. Chem. Minerals* **10** 149